13th International Brick and
Block Masonry Conference
Amsterdam, July 4-7, 2004

A SAW-TOOTH MODEL FOR THE ANALYSIS OF REAL-SCALE MASONRY STRUCTURES

J.G. Rots[1] & S. Invernizzi [2]

Abstract

In real-scale masonry structures the amount of the stored elastic energy is large compared to the fracture energy consumed in crack propagation. Therefore, negative stiffness due to fracture softening arises as a major computational problem, and users have to resort to arc-length or indirect control schemes, which is often inadequate. As an alternative, this paper presents a sequentially linear saw-tooth continuum model which captures the nonlinear response via a series of linear steps. The effectiveness of the method is assessed considering the case of the typical Amsterdam house façade. Comparisons between classical nonlinear analysis and the saw-tooth approach are provided, focussing on masonry façades subjected to tunnelling-induced settlements..

Key Words

Saw-tooth modelling, façade cracking, settlements, tunnelling.

1 Introduction

Negative stiffness due to softening is a major problem in computational modelling of fracture in masonry. It may lead to numerical instability and divergence of the incremental-iterative procedure. This holds especially for the analysis of medium- and large-scale structures (Rots 1994). Cracks in structures are accompanied by dips, ripples, jumps and snap-backs in the load-displacement response. This behavior is typical of un-reinforced structures (e.g. historical facades) where the amount of elastic energy stored in the structure is large compared to the fracture energy consumed in crack or crush propagation, but also of reinforced structures (e.g. reinforced masonry designed to bear seismic loads) where each primary crack gives a release or drop followed by a new ascending portion in the load-displacement curve. To try and solve such problems, users have to resort to arc-length or indirect control schemes which is cumbersome and often inadequate when the peaks are irregular or the snap-backs sharp.

[1] Delft University of Technology, Faculty of Architecture, P.O. Box 5043, 2600 GA Delft, The Netherlands. E-mail: j.g.rots@bk.tudelft.nl
[2] Department of Structural Engineering and Geotechnics Politecnico di Torino, Corso Duca degli Abruzzi 24, 10129 Torino – Italy; also research fellow at Delft University of Technology, Faculty of Architecture. E-mail: stefano.invernizzi@polito.it

As an alternative, this paper presents a sequentially linear saw-tooth continuum model which captures the nonlinear response via a series of linear steps (Rots 2001). The softening stress-strain curve with negative slope is replaced by a saw-tooth diagram of positive slopes, while the incremental-iterative procedure is replaced by a scaled sequentially linear procedure. After a linear analysis, the critical element, i.e. the element for which the stress is most close to the current peak in the saw-tooth diagram, is traced. Next, the stiffness of that element is reduced and the process is repeated. The sequence of critical states governs the global load-displacement response, while the elements with reduced stiffness reveal the softened areas. The advantage is that there is no such thing as 'negative incremental stiffness', as the secant linear (saw-tooth) stiffness is always positive. The analysis always 'converges'. Mesh-size objectivity is achieved by adjusting both the peaks and the ultimate strain of the saw-tooth diagram to the size of the finite elements, keeping the fracture energy invariant (Rots & Invernizzi 2003).
Although the original formulation of the model was able to consider only isotropic damage, the model has been recently improved in order to consider directly the damage anisotropy induced by cracking. This is done by assigning to the cracked element the appropriate orthotropic linear elastic constitutive relation (Rots & Invernizzi 2004).
In the following, after a description of the model, the effectiveness of the method is assessed considering the case of the typical Amsterdam house façade. Comparisons between classical nonlinear analysis and the saw-tooth approach are provided with respect to different loading condition, in particular considering the effect induced by settlement caused by underground tunnelling.

2 SAW-TOOTH SOFTENING MODEL

2.1 Global sequentially linear procedure

The basic idea is to look for the equilibrium configuration via secant approximations with restarts from the origin. The softening diagram is approximated by a saw-tooth curve and linear analyses are carried out sequentially (Rots 2001). This is similar to procedures for fracture analysis on lattices (Schlangen & van Mier 1992, Beranek & Hobbelman 1995), where little beam elements are removed rather than continuum elements reduced.
The global procedure is as follows. The structure is discretized using standard elastic continuum elements with assigned tensile strength. Subsequently, the following steps are carried out:

- Add the external load as a unit load.
- Perform a linear elastic analysis.
- Extract the critical element from the results. The critical element is the element for which the principal tensile stress is closest to its current strength. This principal tensile stress criterion is widely accepted in mode-I fracture mechanics of quasi-brittle materials.
- Calculate the critical global load as the unit load times the current strength divided by stress of the critical element.
- Extract also a corresponding global displacement measure, so that later an overall load-displacement curve can be constructed.
- Reduce the stiffness and strength, i.e. Young's modulus E and tensile strength f_t of the critical element, according to a saw-tooth tensile softening stress strain curve as described in the following.
- Repeat the previous steps for the new configuration, i.e. re-run a linear analysis for the structure in which E and f_t of the previous critical element are reduced.
- …… Repeat again, etc. …….

2.2 Saw-tooth softening model via stepwise isotropic reduction of Young's modulus

The way in which the stiffness and strength of the critical elements are progressively reduced constitutes the essence of the model. A very rough method would be to reduce *E* to zero immediately after the first, initial strength is reached. This elastic perfectly brittle approach, however, is likely to be mesh dependent as it will not yield the correct energy consumption upon mesh refinement (Bazant & Cedolin, 1979). In this study, the consecutive strength and stiffness reduction is based upon the concept of tensile strain softening, which is fairly accepted in the field of fracture mechanics of concrete (Bazant & Oh, 1983).

The tensile softening stress-strain curve is defined by Young's modulus *E*, the tensile strength f_t, the shape of the diagram, e.g. a linear or exponential diagram, and the area under the diagram. The area under the diagram represents the fracture energy G_f divided by the crack band width *h*, which is a discretisation parameter associated with the size, orientation and integration scheme of the finite element. Although there is some size-dependence, the fracture energy can be considered to be a material property. This softening model usually governs nonlinear constitutive behavior in an incremental-iterative strategy. Please note that here we adopt the curve only as a 'mother' or envelope curve that determines the consecutive strength reduction in sequentially linear analysis. In the present study, attention is confined to a linear softening diagram, but extension to any other shape of the diagram is possible. For a linear softening diagram, the ultimate strain ε_u of the diagram reads:

$$\varepsilon_u = \frac{2G_f}{f_t h}. \tag{1}$$

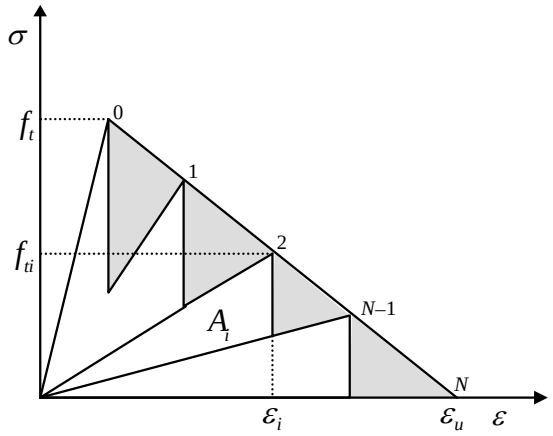

Figure 1. Saw-tooth softening approximation scheme, the underestimated area is shown in gray.

In a sequentially linear strategy, the softening diagram can be imitated by consecutively reducing Young's modulus as well as the strength. Young's modulus can e.g. be reduced according to:

$$E_i = \frac{E_{i-1}}{a}, \qquad \text{for } i = 1 \text{ to } N \tag{2}$$

with *i* denoting the current stage in the saw-tooth diagram, *i*-1 denoting the previous stage in the saw-tooth diagram and *a* being a constant. When *a* is taken as 2, Young's modulus of a critical element is reduced by a factor 2 compared to the previous state. *N*

denotes the amount of reductions that is applied in total for an element. When an element has been critical *N* times, it is removed completely in the next step.
The reduced strength f_{ti} corresponding to the reduced Young's modulus E_i is taken in accordance with the envelope softening stress-strain curve:

$$f_{ti} = \varepsilon_u E_i \frac{D}{E_i + D}, \tag{3}$$

with

$$E_i = \frac{E}{a^i}, \tag{4}$$

and

$$D = \frac{f_t}{\varepsilon_u - \frac{f_t}{E}}, \tag{5}$$

being the tangent to the tensile stress-strain softening curve. Note that this is the softening curve in terms of stress versus *total* strain, i.e. the sum of elastic strain and crack strain of an imagined cracked continuum.
The model always provides a solution: the secant saw-tooth stiffness is always positive, so that ill-conditioning or divergence does not appear in sequentially linear analysis. An advantage of the model is that the regular notions of fracture mechanics, like the principal tensile stress criterion, the envelope strength and fracture energy are maintained which helps in reaching realistic energy consumption and toughness as observed in experiments.

2.3 Mesh regularization

The concept of smeared crack basically assumes that the localized crack is distributed over a continuum finite element, provided that the crack opening δ is equal to the element strain ε times the so called crack band width *h* (for lower-order elements often equal to the element size). In order to achieve mesh-size objectivity, the ultimate strain ε_u in smeared crack models is usually adjusted to *h* according to Eq. (1) for linear softening, Bazant & Oh (1993). In previous works (Rots & Invernizzi, 2003), it appeared that such adjustment is not sufficient to guarantee mesh-size objectivity for the case of the sequentially linear model. In fact, due to the saw-tooth approximation of the softening curve, the dissipated energy is always less than the theoretical one, i.e. the one referring to the smooth 'mother' softening curve. Moreover, the underestimation of the dissipated energy depends not only on the number of teeth, but also on the mesh size, since the ultimate strain depends on the crack band width. When finer meshes are considered, i.e. for a small value of *h*, the slope of the linear softening branch decreases and the area underestimation becomes more important.
In order to provide a correct regularization procedure and achieve mesh independence, it is first of all necessary to provide a useful expression for the actual area beneath the saw-tooth curve. Referring to the scheme in Fig. 1, the formula is the following:

$$A = \sum_{i=0}^{N-1} A_i = \sum_{i=0}^{N-1} \frac{1}{2} \varepsilon_i f_{ti} b_i, \tag{6}$$

where the index *i* refers to the triangular decomposition of the whole area.
The parameter b_i varies depending on the saw-tooth approximation method. In the case of stepwise Young's modulus reduction, it is the following:

$$b_i = \begin{cases} \left(1 - \dfrac{1}{a}\right) & 0 \le i < N-1 \\ 1 & i = N-1 \end{cases}. \tag{7}$$

The basic idea, thus, is to update the tensile strength, or the ultimate strain, or even both, in order to keep the dissipated energy invariant. In other words, the area A^*, under the updated constitutive law, becomes invariant and equal to:

$$A^* = \frac{G_f}{h}. \tag{8}$$

Eq. 8 shows clearly that not only the number of teeth, but also the mesh size (i.e. the crack band width *h*) comes into play.

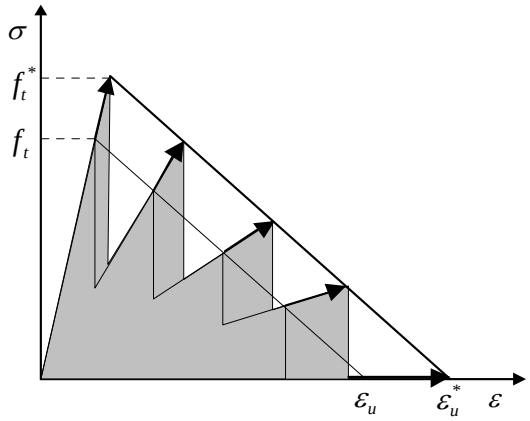

Figure 2. Regularization scheme with both the ultimate strain and the tensile strength update, keeping constant the softening modulus D.

Although in principle different approaches can be followed, it has been proved that the most effective technique is to update both the tensile strength and the ultimate strain. Therefore, the updated strength f_t^* and the ultimate strain ε_t^* will be determined as follow:

$$\begin{cases} f_t^* = k \cdot f_t \\ \varepsilon_t^* = k \cdot \varepsilon_t \end{cases}, \tag{9}$$

where *k* can be determined numerically in such a way that the new area satisfies Eq. 8 (see Fig. 2). After some analytical manipulation of Eq. 8, a closed form expression for the parameter *k* can be obtained:

$$k = \sqrt{\frac{\dfrac{G_f}{h}}{\displaystyle\sum_{i=0}^{N-1} \frac{1}{2} \frac{f_{ti}^2}{E_i} b_i}}. \tag{10}$$

2.4 Anisotropic sequentially linear: fixed cracking

The isotropic reduction of stiffness assumed above, is a rather rough approximation. Therefore, in analogy to the pioneering approach of Rashid (1968), the initial isotropic stress-strain law can be replaced by an orthotropic law upon crack formation, with the axes of orthotropy being determined according to a condition of crack initiation. As far as the present work concerns, the crack plane is kept constant after the crack is nucleated. Moreover, only one crack per element is considered.

Referring to the plane stress situation, and to a local coordinate system oriented parallel to the crack plane, the following constitutive relation is assumed:

$$\begin{Bmatrix} \sigma_{nn} \\ \sigma_{tt} \\ \sigma_{nt} \end{Bmatrix} = \begin{bmatrix} \frac{E_i}{1-\nu^2\frac{E_i}{E}} & \frac{\nu E_i}{1-\nu^2\frac{E_i}{E}} & 0 \\ \frac{\nu E_i}{1-\nu^2\frac{E_i}{E}} & \frac{E}{1-\nu^2\frac{E_i}{E}} & 0 \\ 0 & 0 & \beta G \end{bmatrix} \begin{Bmatrix} \varepsilon_{nn} \\ \varepsilon_{tt} \\ \varepsilon_{nt} \end{Bmatrix}, \tag{11}$$

where n is the normal to the crack, t the crack plane, E_i the reduced Young modulus according to the sequentially linear scheme, and β the so-called shear retention factor. The equation can be rewritten in compact form as follow:

$$\sigma_{nt} = \mathbf{D}_{nt}\varepsilon_{nt}. \tag{12}$$

In addition to Young's modulus, also the shear retention factor and the Poisson ratio decrease with increasing crack opening. In the present implementation a stepwise reduction is assumed:

$$\begin{cases} \beta_i = \dfrac{N-i}{N} \\ \nu_i = \dfrac{N-i}{N} \end{cases}, \quad 0 \le i \le N, \tag{13}$$

where i is the current tooth, and N the number of teeth adopted in the discretization. Given the following transformations for the strain and stress vectors:

$$\begin{cases} \varepsilon_{nt} = \mathbf{T}_\varepsilon(\phi)\varepsilon_{xy} \\ \sigma_{nt} = \mathbf{T}_\sigma(\phi)\sigma_{xy} \end{cases}, \tag{14}$$

eq. 12 can be easily transposed in terms of global stress and strain components by pre- and post-multiplication with the transformation matrices:

$$\sigma_{xy} = \mathbf{T}_\sigma^{-1}(\phi)\mathbf{D}_{ns}\mathbf{T}_\varepsilon(\phi)\varepsilon_{xy}. \tag{15}$$

The improved constitutive law above was implemented in the general sequentially linear scheme.

3 Settlement induced damage in masonry

The boring of tunnels leads to settlements of the soil above the tunnel. These settlements may subsequently cause damage to existing buildings that are located in the settlement trough area. Given a certain shape and magnitude of the settlements trough, the question is: will the settlement lead to unacceptable damage in the existing building? If so, mitigating measures have to be taken, either in the form of improving the tunnelling method by e.g. grouting techniques to reduce settlements, or by taking measures in the buildings by e.g. strengthening techniques or the creation of movements joints at acceptable locations (Rots 2000). This is a major practical concern in urban historical centres where the construction of subways (e.g. the new North-South line right underneath the historical city centre of Amsterdam) and other underground activities are getting more and more important. In the following the typical Amsterdam house Façade will be considered both to emphasize the difficulties that

arise in classical nonlinear fracture analysis and to show the effectiveness of the proposed saw-tooth approach.

3.1 The typical Amsterdam house Façade

An example of a historical masonry façade typical for the western part of the Netherlands is chosen for this study. This numerical study is one part of a joint research project in which the results of the numerical simulation by fracture mechanics will be interpreted and translated into the development of a damage classification system (Netzel 2000) in the near future.

The layout of the masonry façade is shown in Fig. 3a. This is a block of three house units. The total height of the house units is 15 m, starting from the foundation level at 1.5 m below green field, a ground floor level and three levels above that. The length of a house unit is 7 m. The three house units together have a length of 21 m, so that the length over height ratio is 1.4. A uniform thickness of one brick (220 mm) is adopted here for the whole façade. The opening pattern shows two large openings at ground floor and a regular pattern of three window openings at the three floors above. Above the window openings at ground floor, lintels in the form of steel beams are present to distribute the vertical load to either side of the opening.

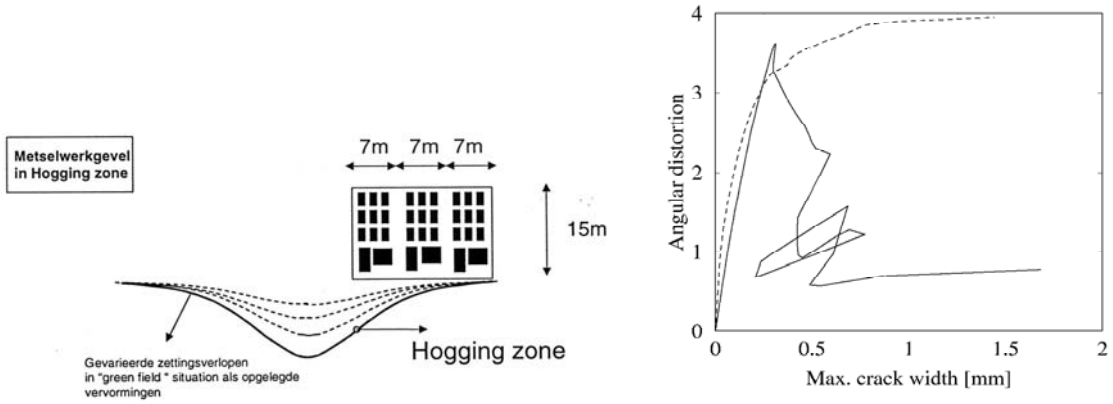

Figure 3. Settlement trough and position of masonry façade in hogging zone (a); Response of the masonry façade. Smeared (dashed) and discrete (drawn) (b).

The façade is located at the point of inflection i.e. in the hogging type situation, which is deemed as the most critical case. The elastic-softening properties of the masonry are assumed as follows. Young's modulus (E) and Poisson's ratio for the masonry are adopted as 6000 N/mm^2 and 0.2 respectively. Fracture properties of the masonry are taken with a tensile strength (f_t) = 0.3 N/mm^2, fracture energy (G_f) = 0.05 N/mm with a linear softening diagram. Mass density of masonry is 2400 kg/m^3.

Fig. 3b shows a result for crack propagation in a large-scale unreinforced masonry facade subjected to settlement (Boonpichetvong & Rots 2003), obtained from classical nonlinear analysis. A global peak is visible and subsequently some sharp peaks in the valley, associated with the crack that discontinuously snapped from window to window. The corresponding deformed meshes are shown, for the smeared and discrete crack simulation, in Fig. 4. Only for discrete cracking, arc-length control provided a solution whereas all smeared trials failed and an unconverged jump-over was found. The difficulty here lies in the large scale (the masonry facade is 180 times larger than e.g. the SEN notched beam benchmark), which gives a large amount of stored elastic energy versus moderate consumption of fracture energy upon crack propagation, resulting in a brittle response and sharp snap-backs.

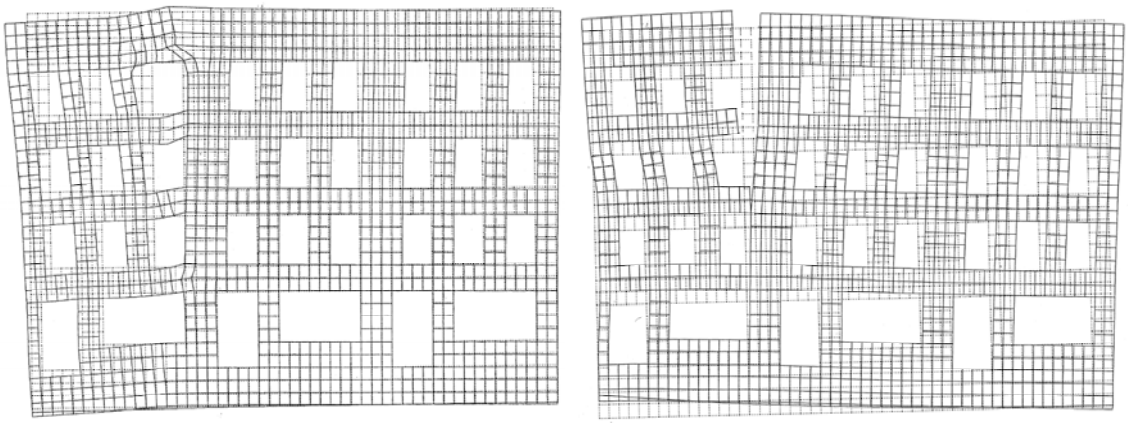

(a) (b)

Figure 4. Incremental displacements diagrams illustrating the fracture localization and through-depth crack at the top: smeared cracking (a); discrete cracking (b).

3.2 Sequentially linear results

A first assessment of the saw-tooth model performance can be illustrated starting from a fictitious proportional loading condition. Here, a vertical point load at the top of the façade, slightly off-center, was taken as an arbitrary example, that relate quite well to the sagging condition. Fig. 5a shows the result in terms of the vertical point load versus displacement. Fig. 5b shows the deformed mesh at one of the final steps of the sequentially linear procedure.

The result reveals the very sharp snap-back behavior, which is found in the sequentially linear fashion without any numerical problems. In the post-peak behavior, we observe four nested snaps, which correspond to the subsequent jumps of the crack from window to window, starting at the bottom and ending at the top of the façade. This is an adequate alternative to the nonlinear analyses summarized in the previous section. A minor aspect is that the present result showed partial stress locking. This was because the mesh consisted of nine-point integrated quadratic eight-node elements. The use of single-point integrated three-node triangles will solve that problem, as a single integration point governs the total element behaviour and false stress transfer is impossible.

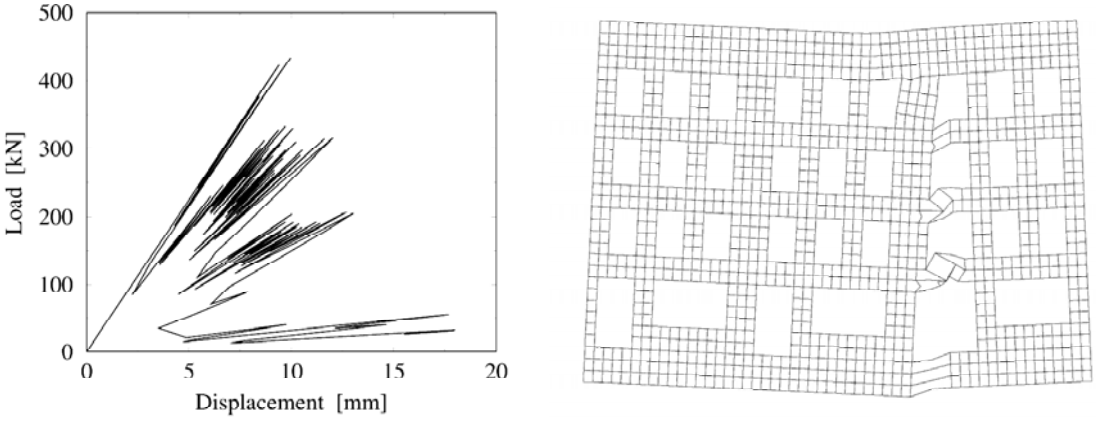

(a) (b)

Figure 5. Load-displacement curve (a), and incremental displacement (b) for sequentially linear analysis of masonry façade under point load.

3.3 Non proportional loading

This section considers a masonry façade subjected to settlements. A ten-teeth isotropic saw-tooth model with *a*=2, *n*=10 is used. A difficulty with this problem is that it involves a non-proportional loading scheme. First, dead weight is added and subsequently the settlement trough. It appears that non-proportional loading for sequentially linear analysis on lattices or other structures has not yet received much attention in literature. A way to solve this is to run sequentially linear analyses for the various load sets in an incremental fashion. First, the first load set is analyzed sequentially linear and the results are frozen. From this frozen situation, the sequentially linear analysis for the second load set is undertaken whereby initial stresses, strains and displacements are accounted for. This process requires the new critical element for the second (or subsequent) load set to be determined again on the basis of the principal stress criterion. The principal stresses can be derived from:

$$\begin{cases} \sigma_{xx} = \sigma_{xx,0} + \lambda \Delta\sigma_{xx} \\ \sigma_{yy} = \sigma_{yy,0} + \lambda \Delta\sigma_{yy} \\ \sigma_{xy} = \sigma_{xy,0} + \lambda \Delta\sigma_{xy} \end{cases}, \tag{14}$$

for a plane stress situation, with $_0$ referring to the preceding load set(s) and Δ referring to the increment of the current load set. The set of Eq. 14 is of quadratic type and some algebraic manipulation provides a couple of cumbersome closed form solutions for the sequentially linear multiplier, where only the positive one can be considered. It is worth noting that when $\Delta\sigma_{xy} = \sqrt{\Delta\sigma_{xx} \cdot \Delta\sigma_{yy}}$ special expressions of the solution must be considered to avoid singularity.

This approach has been implemented in the isotropic sequentially linear procedure, while an extension to the orthotropic case is currently under development.

The deformed mesh in Fig. 6a shows the obtained fracture pattern when the façade is in the hogging region of the settlement trough. Fig. 6b shows the zoomed diagram describing the evolution of the angular distortion as a function of the maximum crack width, with the resulting snap behavior that accompanies the sudden crack propagation across the façade. Although further analyses are still under study, the results provide a stable alternative to the jumpy response of Fig. 3b.

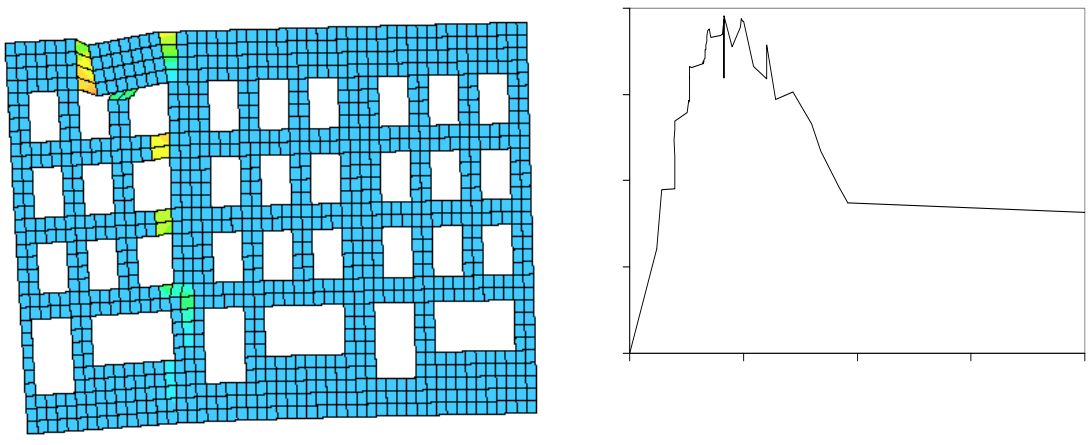

(a) (b)

Figure 6. Deformed mesh in the hogging region of the settlement trough. The colors emphasize the crack path across the façade (a). Load-displacement curve for the masonry façade subjected to non-proportional load (b).

4 Conclusions

A sequentially linear continuum model for fracture in masonry has been proposed. The model approximates an envelope softening stress-strain curve by a saw-tooth diagram. In each linear analysis, a critical element is traced by comparing element stress with current element strength, i.e. with the current peak in the saw-tooth diagram. Next the stiffness and strength of the critical element are reduced according to the subsequent tooth of the diagram, and the process is repeated.

The charm of this model is that words like iteration, ill-conditioning and divergence do not appear in the vocabulary. The advantage of the model especially appears in case of brittle, complex snap-back behavior as was illustrated by large-scale analysis of a masonry façade.

Moreover, settlement damage prediction by means of a fracture mechanics approach is presented in this paper, from which useful and practical design information can be derived. We conclude that the performance of the smeared crack models in simulating settlement damage prediction for masonry yields some limitations, while the sequentially linear approach provides a valuable and promising alternative.

5 Acknowledgements

Financial support from Delft Cluster, COB and the Netherlands Technology Foundation STW is acknowledged. The research was carried out using an adapted version of DIANA.

References

Bazant, Z.P., Cedolin, L., 1979, Blunt crack band propagation in finite element analysis. ASCE *J. Engineering Mechanics Division* 105(2): 297-315.

Bazant, Z.P.,Oh, B.H., 1983. Crack band theory for fracture of concrete. *Materials and Structures* 16(93): 155-177.

Boonpichetvong M, Rots JG., 2003, Settlement damage of masonry buildings in soft-ground tunneling. . *Computational modelling of concrete structures; Proc. EURO-C 2003*. Eds. R. de Borst et al. : 655-665.

Netzel, H., 2000, Guideline on prediction of damage to buildings, part of *Guidelines for the design of bored tunnels for road and rail infrastructure*, Center for Underground Structures CUR/COB, committee L500, committee L540, CUR/COB, Gouda, the Netherlands.

Rots, J.G. (Ed.), 1994, Structural masonry - An experimental/numerical basis for practical design rules. CUR report 171, CUR, Gouda (in Dutch). English version published by Balkema, Rotterdam in 1997.

Rots, J.G., 2000, Settlement damage predictions for masonry, In L.G.W. Verhoef and F.H. Wittmann (eds), *Maintenance and restrengthening of materials and structures - Brick and brickwork*, Proc. Int Workshop on Urban heritage and building maintenance: 47-62.

Rots, J.G., 2001, Sequentially linear continuum model for concrete fracture. In de Borst R., Mazars J., Pijaudier-Cabot G., van Mier J.G.M. (eds), *Fracture Mechanics of Concrete Structures*: 831-839. Lisse: Balkema

Rots, J.G., Invernizzi S., 2003, Regularized saw-tooth softening, In Bicanic N., de Borst R., Mang H., Meschke G. (eds), *Computational Modelling of Concrete Structures*: 599-617. Lisse: Balkema.

Rots, J.G., Invernizzi S., 2004, Saw-tooth softening/stiffening model, in *Proceedings of the Fifth International Conference on Fracture Mechanics of Concrete and Concrete Structures FRAMCOS-5,* April 12-16, Vail, Colorado.

Schlangen, E., van Mier J.G.M., 1992, Experimental and numerical analysis of micro-mechanisms of fracture of cement-based composites. *Cement & Concr Comp* 14: 105-118.

Beranek, W.J., Hobbelman, G.J., 1995, 2D and 3D-Modelling of concrete as an assemblage of spheres: revaluation of the failure criterion. In Wittmann F.H. (ed.), *Fracture mechanics of concrete structures. Proc. FRAMCOS-2*: 965-978. Freiburg: Aedificatio.

Rashid, Y.R. 1968. Analysis of prestressed concrete pressure vessels, *Nuclear Engng. And Design* 7(4): 334-344.